BIOCHEMISTRY
including biophysical chemistry & molecular biology

Article

pubs.acs.org/biochemistry

Predictive Model for Epoxide Hydrolase-Generated Stereochemistry in the Biosynthesis of Nine-Membered Enediyne Antitumor Antibiotics

Geoffrey P. Horsman,[†,⊥] Anna Lechner,[‡] Yasuo Ohnishi,[§] Bradley S. Moore,[‡] and Ben Shen*[,†,∥]

[†]Division of Pharmaceutical Sciences, University of Wisconsin−Madison, Madison, Wisconsin 53705, United States

[‡]Scripps Institution of Oceanography and the Skaggs School of Pharmacy and Pharmaceutical Sciences, University of California−San Diego, La Jolla, California 92093, United States

[§]Department of Biotechnology, University of Tokyo, Tokyo, Japan

[∥]Department of Chemistry and Department of Molecular Therapeutics, Natural Products Library Initiative at The Scripps Research Institute, The Scripps Research Institute, Jupiter, Florida 33458, United States

Supporting Information

ABSTRACT: Nine-membered enediyne antitumor antibiotics C-1027, neocarzinostatin (NCS), and kedarcidin (KED) possess enediyne cores to which activity-modulating peripheral moieties are attached via (*R*)- or (*S*)-vicinal diols. We have previously shown that this stereochemical difference arises from hydrolysis of epoxide precursors by epoxide hydrolases (EHs) with different regioselectivities. The inverting EHs, such as SgcF, hydrolyze an (*S*)-epoxide substrate to yield an (*R*)-diol in C-1027 biosynthesis, whereas the retaining EHs, such as NcsF2 and KedF, hydrolyze an (*S*)-epoxide substrate to yield an (*S*)-diol in NCS and KED biosynthesis. We now report the characterization of a series of EH mutants and provide a predictive model for EH regioselectivity in the biosynthesis of the nine-membered enediyne antitumor antibiotics. A W236Y mutation in SgcF increased the retaining activity toward (*S*)-styrene oxide by 3-fold, and a W236Y/Q237M double mutation in SgcF, mimicking NcsF2 and KedF, resulted in a 20-fold increase in the retaining activity. To test the predictive utility of these mutations, two putative enediyne biosynthesis-associated EHs were identified by genome mining and confirmed as inverting enzymes, SpoF from *Salinospora tropica* CNB-440 and SgrF (SGR_625) from *Streptomyces griseus* IFO 13350. Finally, phylogenetic analysis of EHs revealed a familial classification according to inverting versus retaining activity. Taken together, these results provide a predictive model for vicinal diol stereochemistry in enediyne biosynthesis and set the stage for further elucidating the origins of EH regioselectivity.

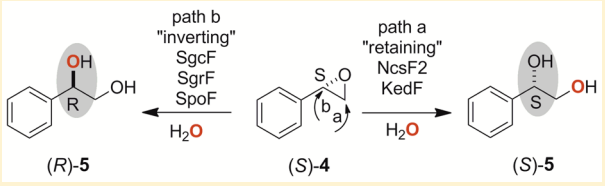

The exponential growth of genomic data in the past decade has provided a great deal of information about microbial natural product biosynthesis and ushered in an era of genome mining to identify new molecules of potential therapeutic value.[1,2] However, it has also highlighted challenges associated with accurately predicting chemical structures from genetic information.[3] For example, many biosynthetic clusters possess unknown genes, and even genes with high sequence similarity may encode enzymes catalyzing unexpected reactions.[4,5]

The enediyne antitumor antibiotics are a family of microbial natural products that exemplify this information gap between genes and chemical structures. Enediynes are potent cytotoxic compounds in clinical use as anticancer agents that function by a unique DNA cleavage mechanism.[6−9] This unusual biological activity originates from the fascinating chemical structure composed of a central enediyne core and activity-modulating peripheral moieties (Figure 1A). Several biosynthetic gene clusters have been sequenced and characterized, leading to a proposed convergent biosynthesis in which each of the peripheral moieties is assembled prior to attachment to the central core.[10−14] Although these clusters have revealed a great deal about peripheral group biosynthesis,[15,16] the assembly and modification of the enediyne core itself remains poorly understood. For instance, three of the five genes that comprise the conserved "enediyne cassette" are of unknown function, and most of the genes that modify the core have not been identified.[17,18]

Despite the difficulties associated with characterizing the enediyne core biosynthetic machinery, we have successfully identified genes involved in modifying a putative nine-membered enediyne core intermediate. Each of the three nine-membered biosynthetic gene clusters (C-1027 (**1**), neocarzinostatin (NCS, **2**), and kedarcidin (KED, **3**)) encode an epoxide hydrolase (EH), SgcF, NcsF2, and KedF, respectively, which are proposed to generate a vicinal diol intermediate from an epoxide precursor.[19−21] Intriguingly, the diol stereochemistry differs among these enediynes, resulting in an (*R*)-diol for C-1027 in comparison to (*S*)-diols for NCS and

Received: May 6, 2013
Revised: June 7, 2013
Published: July 11, 2013

dx.doi.org/10.1021/bi400572a | *Biochemistry* 2013, 52, 5217−5224

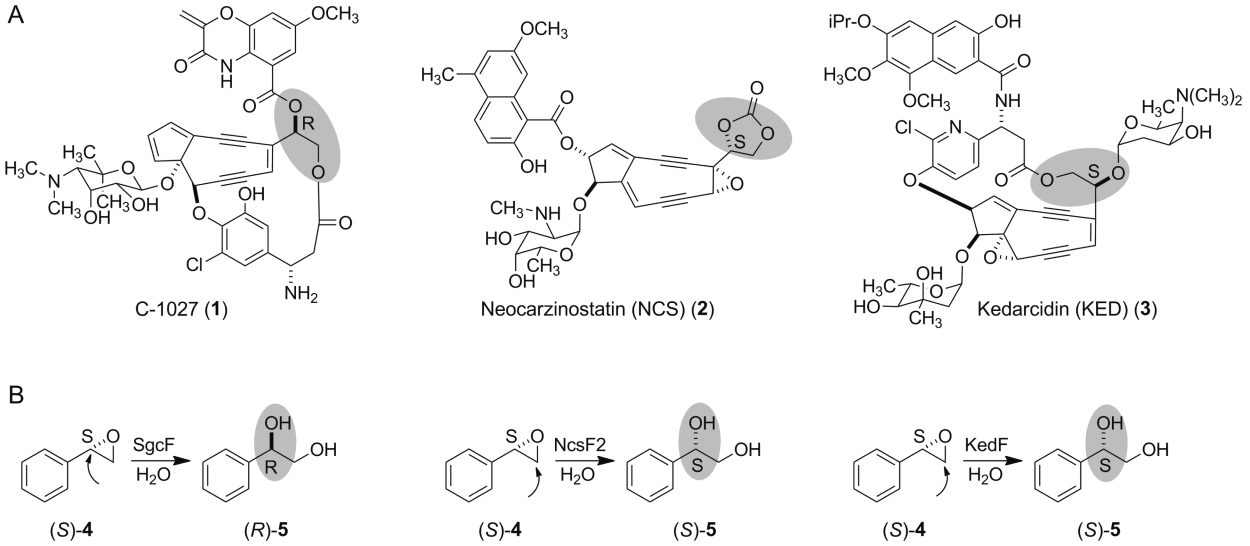

Figure 1. (A) Structures of the enediyne chromophores of chromoproteins C-1027 (**1**), neocarzinostatin (NCS, **2**), and kedarcidin (KED, **3**), with their respective (*R*)- and (*S*)-vicinal diol stereochemistry highlighted. (B) Stereochemical outcome from the hydrolysis of (*S*)-**4** catalyzed by SgcF, NcsF2, and KedF, which are the respective EHs from the **1**, **2**, and **3** biosynthetic machinery. Arrows indicate the regioselectivity of epoxide ring-opening in each enzyme reaction.

KED (Figure 1A). Biochemical characterization using styrene oxide (**4**) as a substrate mimic demonstrated catalytic activities consistent with a biosynthetic scheme in which an (*S*)-epoxide is directed to different stereochemical outcomes by EHs with differing regioselectivities (Figure 1B). Specifically, SgcF acts as an inverting enzyme by regioselectively catalyzing the net addition of water at the more hindered carbon of (*S*)-**4** to invert the stereochemistry, yielding (*R*)-1-phenyl-1,2-ethanediol ((*R*)-**5**). In contrast, the retaining enzymes NcsF2 and KedF attack at the less-hindered carbon of (*S*)-**4** to afford (*S*)-1-phenyl-1,2-ethanediol ((*S*)-**5**), retaining the (*S*)-configuration.

These three highly related EHs present an outstanding opportunity to probe the basis for the regioselectivity in enediyne biosynthesis and to bioinformatically assign the stereochemical configuration of new enediynes. Herein, we identify a rare EH tyrosine-to-tryptophan mutation in SgcF that influences regioselectivity. Genome mining for this mutation in enediyne biosynthesis-associated EHs identified two additional enzymes (SpoF from *Salinospora tropica* CNB-440[22] and SgrF from *Streptomyces griseus* IFO 13350[23]) that were biochemically confirmed as inverting EHs. The predictive utility of this model was expanded by the observed phylogenetic separation of enediyne biosynthesis-associated EHs into inverting and retaining groups. In addition, the location of *spoF* within the gene cluster encoding the biosynthesis of the (*R*)-diol-containing sporolides suggests that this sequence-based model may be used to predict the stereochemical configuration of proposed nine-membered enediynes identified from genome sequencing projects.

MATERIALS AND METHODS

General Information. DNA sequencing and oligonucleotide synthesis were performed by the University of Wisconsin-Madison Biotechnology Center. Chemicals, including racemic (*R*)- and (*S*)-styrene oxide and racemic (*R*)- and (*S*)-1-phenyl-1,2-ethanediol, were purchased from Sigma-Aldrich (St. Louis, MO). Dithiothreitiol (DTT) was purchased from Research Products International (Mt. Prospect, IL) and Complete Protease Inhibitor was purchased from Roche Applied Science (Indianapolis, IN). Media components and buffers were from Fisher Scientific (Pittsburgh, PA). PCR amplification used Pfx polymerase (Invitrogen, Carlsbad, CA), and 3′-A overhangs were added with Taq polymerase from Invitrogen for 10 min at 72 °C prior to subcloning into pGEM-T Easy (Promega, Madison, WI). Sequence alignments and phylogenetic analyses were performed with ClustalX, and phylogenetic trees were drawn using Hypertree or MEGA.[24] The homology models were constructed using SWISS-MODEL.[25] Primers (Table S1), plasmids (Table S2), and the sequence comparison of the five EHs (Table S3) are summarized in the Supporting Information. Sequence alignment of the EHs (Figure S1), SDS-PAGE analysis of the purified EHs (Figure S2), and curve-fitted steady-state kinetic data (Figure S3) are also provided in the Supporting Information.

Cloning of the *sgrF* and *spoF* Genes That Encode Putative EHs. The *sgrF* gene was PCR amplified from plasmid TGL_028_D08 using primers SGR625-NdeI-F and SGR625-XhoI-R (Table S1). Plasmid TGL_028_D08 contains ∼12 kb of *Streptomyces griseus* IFO 13 350 genomic DNA[23] inserted into the HincII site of the pTS1 vector (Nippon Genetech, Tokyo, Japan) and includes the EH gene *SGR625* that we have renamed *sgrF*. The *sgrF* PCR product possessed added 3′ XhoI and 5′ NdeI restriction sites together with the DNA encoding the N-terminal amino acid sequence (MAH_6VD_4K) of the pCDF-2 Ek/LIC vector (Novagen, Madison WI) to generate a protein with N-terminal features identical to SgcF produced from pBS1096.[19] This PCR product was then cloned into pGEM-T Easy (Promega, Madison, WI) to yield pBS1118, which was confirmed by DNA sequencing. The *sgrF* gene was then cloned as an NdeI−XhoI fragment into pET29 (Novagen, Madison, WI) to afford the *sgrF* expression construct pBS1119. The *spoF* gene was cloned using the identical strategy by PCR amplification from *Salinospora tropica* CNB-440 genomic DNA[22] using primers SpoF-NdeI-F and SpoF-XhoI-R (Table S1). The PCR product was cloned into pGEM-T Easy to make pBS1120, from which the NdeI−XhoI fragment was transferred into pET29 to produce the *SpoF* expression construct pBS1121.

dx.doi.org/10.1021/bi400572a | *Biochemistry* 2013, 52, 5217−5224

Mutant SgcF (W236Y). Site-directed mutagenesis was carried out by PCR overlap extension from the pBS1096 template.[19] To generate the SgcF (W236Y) mutant, two sets of primers (SgcF-W236Y-F + SgcF-W236Y-mutR; SgcF-W236Y-mutF + SgcF-W236Y-R) (Table S1) were used to PCR amplify two SgcF fragments of 417 and 170 bp, respectively, that overlapped at the mutation site located in primers SgcF-W236Y-mutF and SgcF-W236Y-mutR. The two PCR fragments were then used as template to amplify the entire 566 bp fragment containing the mutation using flanking primers SgcF-W236Y-F and SgcF-W236Y-R (Table S1). This fragment was cloned into pGEM-T Easy to afford pBS1122, which was confirmed by DNA sequencing. A 510 bp AatII−SmaI fragment containing the mutation was then cloned from pBS1122 back into pBS1096 to produce expression construct pBS1123 (Table S2).

Mutant SgcF (W176L). The same mutagenic strategy as above was employed, but mutagenic primers SgcF-W176L-mutF and SgcF-W176L-mutR (Table S1) were used. The resulting 566 bp product of the PCR overlap extension was cloned into pGEM-T Easy to yield pBS1124, which was confirmed by sequencing. The 510 bp fragment possessing the W176L mutation was cloned back into pBS1096 to afford expression construct pBS1125 (Table S2).

Mutant SgcF (Q237M). The above strategy was used with primers SgcF-Q237M-mutF and SgcF-Q237M-mutR (Table S1), and the 566 bp product was cloned into pGEM-T Easy to create pBS1126. The 510 bp AatII−SmaI fragment with the Q237M mutation was cloned back into pBS1096 to generate expression construct pBS1127 (Table S2).

Mutant SgcF (W236Y/Q237M). The above PCR overlap extension strategy was employed, but pBS1123 was used as the template with primers SgcF-W236Y/Q237M-mutF and SgcF-W236Y/Q237M-mutR (Table S1). The mutated PCR product was cloned into pGEM-T Easy to make pBS1128, from which the AatII−SmaI fragment was moved back into pBS1096 to afford expression construct pBS1129 (Table S2).

Mutants SgcF (W176L/Q237M) and SgcF (W176L/W236Y/Q237M). The 315 bp AatII−XcmI fragment from the W176L-containing pBS1124 was cloned into the same sites of Q237M-containing pBS1126 and W236Y/Q237M-containing pBS1128 to afford pBS1130 and pBS1131, respectively. The AatII−SmaI fragments from W176L/Q237M-containing pBS1130 and W176L/W236Y/Q237M-containing pBS1131 were cloned back into pBS1096 to yield expression constructs pBS1132 and pBS1133, respectively (Table S2).

Mutant NcsF2 (Y235W). PCR overlap extension was performed as above, but pBS5042[20] was used as the template with two primer sets (NcsF2-Y235W-F + NcsF2-Y235W-mutR; NcsF2-Y235W-mutF + NcsF2-Y235W-R) (Table S1) to yield respective overlapping PCR fragments of 410 and 470 bp. These fragments were used as the template to amplify the entire 860 bp mutated fragment using flanking primers NcsF2-Y235W-F and NcsF2-Y235W-R (Table S1), which was then cloned into pGEM-T Easy to make pBS5043. After confirmation by DNA sequencing, a 490 bp PstI−AatII fragment was cloned from pBS5043 back into the *ncsF2*-containing expression plasmid pBS5042 to afford pBS5044 (Table S2).

Mutant NcsF2 (L176W). The same mutagenic strategy as for NcsF2 (Y235W) was employed but with mutagenic primers NcsF2-L176W-mutF and NcsF2-L176W-mutR (Table S1). The resulting 860 bp product of the PCR overlap extension was cloned into pGEM-T Easy to yield pBS5045 and confirmed by sequencing. The 490 bp PstI−AatII fragment possessing the L176W mutation was cloned back into pBS5042 to afford expression construct pBS5046 (Table S2).

Mutant NcsF2 (M236Q). The above strategy was used with primers NcsF2-M236Q-mutF and NcsF2-M236Q-mutR (Table S1), and the 860 bp product was cloned into pGEM-T Easy to create pBS5047. The 490 bp PstI−AatII fragment with the M236Q mutation was cloned back into pBS5042 to generate expression construct pBS5048 (Table S2).

Mutant NcsF2 (Y235W/M236Q). The above PCR overlap-extension strategy was employed, but pBS5044 was used as the template with primers NcsF2-Y235W/M236Q-mutF and NcsF2-Y235W/M236Q-mutR (Table S1). The mutated PCR product was cloned into pGEM-T Easy to make pBS5049, from which the PstI−AatII fragment was moved back into pBS5042 to afford expression construct pBS5050 (Table S2).

Mutants NcsF2 (L176W/M236Q) and NcsF2 (L176W/Y235W/M236Q). The 490 bp PstI−AatII fragment from either M236Q-containing pBS5047 or Y235W/M236Q-containing pBS5049 was cloned into the same site of L176W-containing pBS5046 to afford expression constructs pBS5051 and pBS5052, respectively (Table S2).

Overproduction and Purification of EHs. The transformation of the various constructs expressing wild-type EHs and their variants (Table S2) into *Escherichia coli* BL21(DE3), their overproduction, and the purification of the resultant EHs were performed as previously described.[19]

EH Activity Assays toward Styrene Oxide. HPLC assays were performed in 200 μL reaction mixtures containing 2 mM styrene oxide and 50 mM potassium phosphate buffer, pH 8.0, following a previously described procedure.[19] Thus, the reaction was initiated by adding 50 μM enzyme followed by incubation at 25 °C for 1 h. The reaction was quenched by extraction with ethyl acetate (3 × 200 μL), and the organic extract was evaporated to dryness in a speed-vac. The resulting residue was dissolved in 50 μL of acetonitrile, and 25 μL of this was analyzed by HPLC. Control reactions without enzyme were carried out in parallel. For general activity assays, the substrate used was racemic styrene oxide, and HPLC was performed with a Varian HPLC system equipped with Prostar 210 pumps, a photodiode array detector, and an Alltech Alltima C18 column (5 μm, 4.6 × 250 mm^2, Grace Davison Discovery Sciences, Deerfield, IL) using a 12 min linear gradient from 10 to 50% acetonitrile in water. Chiral HPLC was performed on an Agilent 1260 HPLC system equipped with a Chiralcel OD-H column (5 μm, 4.6 × 250 mm^2, Grace Davison Discovery Sciences) using a 70 min isocratic elution with 2.5% isopropanol in *n*-hexane.

Steady-State Kinetics of EHs. Enzyme kinetic assays were performed as previously described.[19] Briefly, the hydrolysis of each enantiomer of styrene oxide with each enzyme was kinetically characterized by adding an appropriate amount of enzyme to a 1 mL reaction mixture containing 10 μL of 300 mM sodium periodate in DMF, 20 μL of an appropriate concentration of styrene oxide, and 50 mM sodium phosphate buffer at pH 8.0. Product formation was monitored by the increase in absorbance at 290 nm over time at 25 °C. Equations for Michaelis−Menten kinetics with or without substrate inhibition were fit to the data by nonlinear regression analysis of the initial velocity versus substrate concentration using the online curve-fitting tools at http://zunzun.com.

RESULTS AND DISCUSSION

Sequence Comparisons to Identify Regioselectivity Determinants. Sequence alignments between the three characterized enediyne biosynthesis-associated EHs (SgcF, NcsF2, and KedF) revealed highly similar enzymes with 62−64% identity and 74−75% similarity (Table S3). These enzymes possess features typical of canonical EHs of the α/β-hydrolase fold family,[26] including most notably the presence of two tyrosine residues that serve to anchor and activate the epoxide toward nucleophilic attack (Figures 2 and S1).

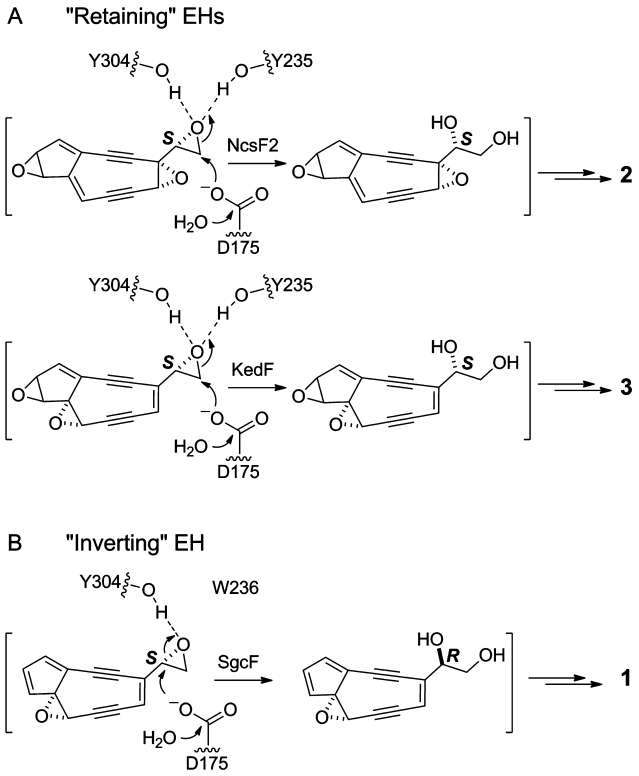

Figure 2. Comparison of the proposed reactions catalyzed by (A) the retaining EHs NcsF2 and KedF, which possess a full complement of two conserved tyrosine residues, and (B) the inverting EH SgcF in which one of the tyrosines is replaced by tryptophan. The square parentheses denote that the reaction is hypothetical.

Strikingly, although the retaining enzymes NcsF2 and KedF possess both of these tyrosine residues (Y235 and Y304, Figure 2A), one of these tyrosines has been replaced by tryptophan (W236) in the inverting enzyme SgcF (Figures 2B and S1). The substitution of this key conserved residue in an inverting enzyme of otherwise high sequence similarity with retaining enzymes suggests that this substitution may influence the regioselectivity of the enzyme reaction (Figure 2). Intriguingly, a role for tyrosine residues in directing regioselective epoxide ring-opening by EHs has been proposed on the basis of molecular dynamics simulations.[27] Therefore, we were motivated to study the role of the SgcF Y236W substitution in directing EH regioselectivity (i.e., inversion versus retention).

Characterization of the Regioselectivity of the SgcF (W236Y) Variant. To assess the effect of the tryptophan substitution on regioselectivity we constructed the SgcF (W236Y) variant possessing the full complement of two tyrosine residues. If these two tyrosines are important for retaining activity, then installation of this canonical active-site feature should increase its activity. Similarly, the NcsF2 (Y235W) variant was constructed to determine if this mutation could increase the inverting activity of NcsF2. The His_6-tagged variant enzymes were purified, and their activity toward (±)-**4** was assessed by HPLC. Unexpectedly, although both variants were soluble, only SgcF (W236Y) was active, demonstrating that the Y235W mutation severely disrupted NcsF2 catalysis. The regioselectivity of the SgcF (W236Y)-catalyzed hydrolysis of (*R*)- and (*S*)-**4** was then characterized by chiral HPLC analysis of the diol products (Figure 3). Consistent with a role for this residue in directing regioselectivity, the retaining activity of the SgcF (W236Y) variant toward (*S*)-**4** increased 3-fold relative to wild-type SgcF. Specifically, only 1.7% of SgcF catalytic turnovers (~1 in 60) produced (*S*)-**5** from (*S*)-**4**, whereas this was increased to 4.6% of turnovers (~1 in 20) for SgcF (W236Y) (Table 1 and Figure 4). Similarly, the W236Y mutation increased the retaining activity toward the (*R*)-**4** substrate to obtain (*R*)-**5** from 83% of turnovers relative to 70% in wild-type SgcF. Thus, although the SgcF (W236Y) variant was only modestly more retaining toward (*S*)-**4**, this mutation clearly affects regioselectivity.

Structure-Based Assessment of Additional Potential Regioselectivity Determinants. The modest change in regioselectivity accompanying the W236Y mutation suggests that other mutations act in concert with W236 to repurpose the SgcF active site for inversion. To search for such determinants, we revisited the sequence comparisons looking for residues that were conserved only between the retaining enzymes NcsF2 and KedF but not in the inverting enzyme SgcF. We elected to limit our search to amino acids in the active site by using a homology model based on the crystal structure of EH from *Aspergillus niger* (AnEH), which is 30% identical to SgcF and NcsF2 (Figure 5). This served to focus our efforts on two additional active-site residue positions occupied by similar amino acids in the retaining enzymes compared to the inverting enzyme SgcF: (i) the residue adjacent to W236 in SgcF is Q237, whereas the residue adjacent to Y235 in NcsF2 and KedF is M236 and (ii) position 176 is occupied by the aromatic amino acid W in SgcF but by hydrophobic residues L and A in NcsF2 and KedF, respectively (Figures 5 and S1).

Combinatorial libraries of SgcF and NcsF2 variants were prepared and tested for regioselectivity. The mutagenesis at each of these three residues individually and in combination were prepared to afford libraries of (i) SgcF variants possessing NcsF2-like amino acid substitutions and (ii) NcsF2 variants possessing SgcF-like substitutions. Thus, a total of seven variants for each enzyme were created to explore all possible combinations. Although the additional NcsF2 variants and the SgcF (W176L) variant were insoluble, two SgcF variants, Q237M and W236Y/Q237M, could be produced and purified as soluble enzymes (Figure S2A). The regioselectivity toward both (±)-**4** was then assessed using chiral HPLC (Figure 3). Although the single mutation Q237M had almost no effect on regioselectivity toward (*S*)-**4**, the combination of substitutions in the W236Y/Q237M variant produced a 21-fold increase in the retaining activity to 36%, which is more than 1 in 3 enzyme turnovers (Table 1, Figures 3A panel IV and 4). The W236Y/Q237M mutation significantly increased the retaining activity of SgcF toward both (*R*)- and (*S*)-**4** such that it becomes more "NcsF2-like" (Figure 4). Interestingly, the inability of NcsF2 to accept SgcF-like mutations, in contrast to the relative ease with

dx.doi.org/10.1021/bi400572a | *Biochemistry* 2013, 52, 5217−5224

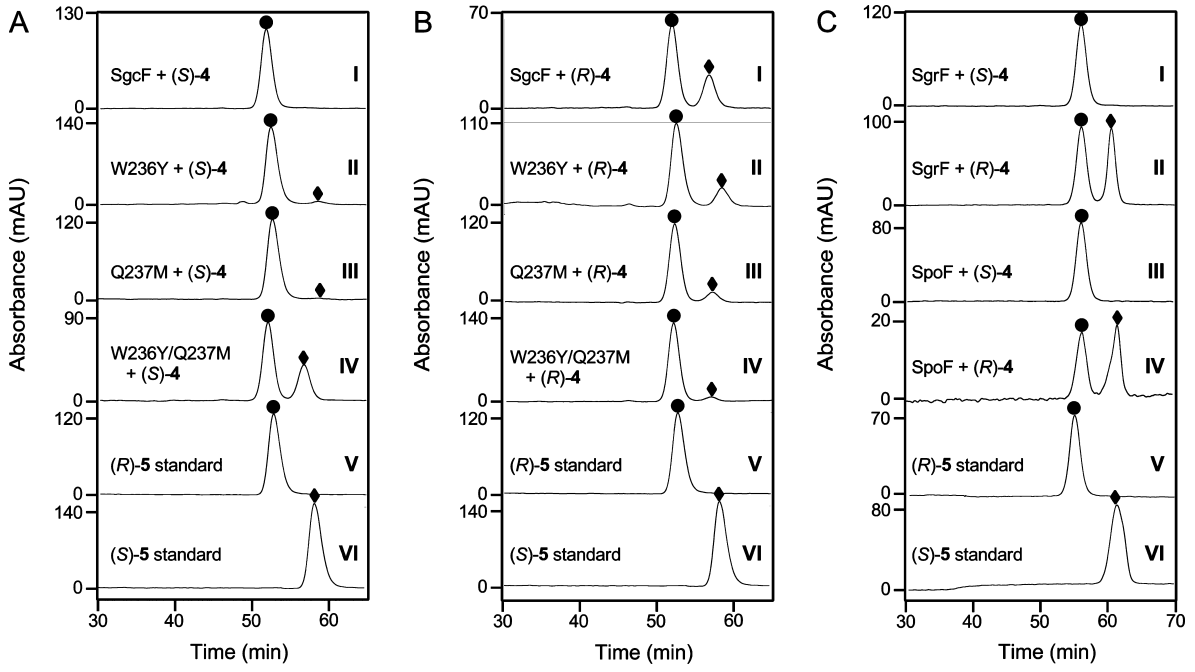

Figure 3. Chiral HPLC analysis of the stereochemistry of **5** generated by EHs. (A) Products of the (*S*)-**4** hydrolysis catalyzed by SgcF for wild-type (I), W236Y (II), Q237M (III), and W236Y/Q237M (IV). (B) Products of the (*R*)-**4** hydrolysis catalyzed by SgcF for wild-type (I), W236Y (II), Q237M (III), and W236Y/Q237M (IV). (C) Products of hydrolysis of (*S*)-**4** by SgrF (I), (*R*)-**4** by SgrF (II), (*S*)-**4** by SpoF (III), and (*R*)-**4** by SpoF (IV). In panels A–C, traces V and VI represent (*R*)-**5** (●) and (*S*)-**5** (♦) standards, respectively.

Table 1. Regioselectivity of SgcF Wild-Type and Variants towards (*R*)- and (*S*)-4[ab]

	(*R*)-**4** substrate			(*S*)-**4** substrate		
EH	% ee of (*R*)-**5**	% retained	$\Delta\Delta G^{\ddagger}$ (kJ/mol)[b]	% ee of (*R*)-**5**	% retained	$\Delta\Delta G^{\ddagger}$ (kJ/mol)[c]
SgcF wild-type	40.1 ± 2.5	70	−2.10	96.6 ± 0.1	1.7	−10.03
SgcF (W236Y)	65.6 ± 3.6	83	−3.90	90.8 ± 3.4	4.6	−7.62
SgcF (Q237M)	79.6 ± 5.2	90	−5.44	95.9 ± 0.6	2.1	−9.58
SgcF (W236Y/Q237M)	88.5 ± 0.5	94	−6.93	28.4 ± 4.9	36	−1.45

[a]Reported as the percent enantiomeric excess (% ee) of the product (*R*)-**5**, % retaining activity, and the difference in free energy of activation between hydrolysis at each epoxide carbon ($\Delta\Delta G^{\ddagger}$). [b]Errors represent the standard deviations of three measurements. [c]Calculated according to the equation $\Delta\Delta G^{\ddagger} = -RT \ln[\text{major diol}]/[\text{minor diol}]$.[29,30]

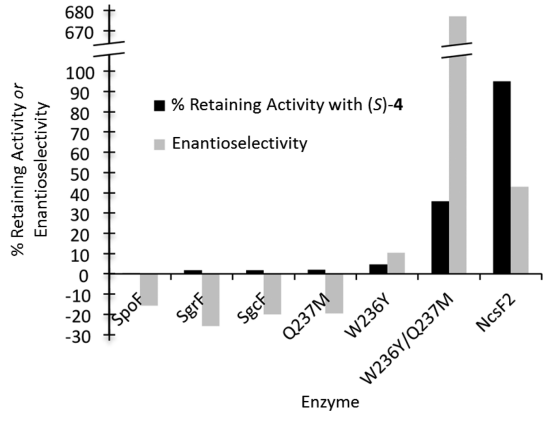

Figure 4. Comparison of the regio- and enantioselectivities of EHs. Regioselectivity is depicted as the percent of turnovers that result in the retention of stereochemistry of substrate (*S*)-**4**. Enantioselectivity describes the ratio of specificity constants for (*R*)-**4** versus (*S*)-**4**. Positive values represent an enzyme preference for (*R*)-**4** [$(k_{cat}/K_m)_R/(k_{cat}/K_m)_S$], and negative values denote a preference for (*S*)-**4** [$-(k_{cat}/K_m)_S/(k_{cat}/K_m)_R$].

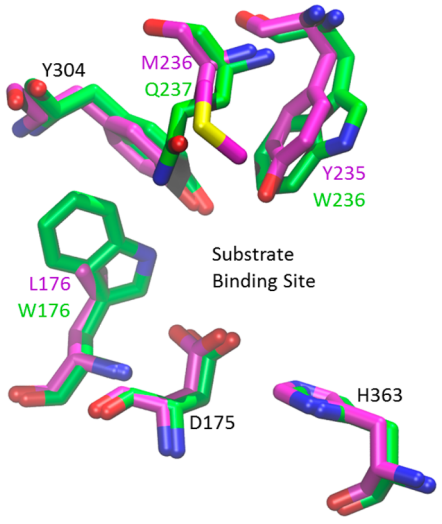

Figure 5. Comparison of NcsF2 (magenta CPK colors) and SgcF (green CPK colors) active sites based on a homology model with AnEH (PDB ID 1qo7).

dx.doi.org/10.1021/bi400572a | *Biochemistry* 2013, 52, 5217–5224

Table 2. Steady-State Kinetic Parameters for EHs towards (*R*)- and (*S*)-4 as Substrates

	(*R*)-4 substrate			(*S*)-4 substrate			
EH	k_{cat} (min^{-1})	K_m (mM)	k_{cat}/K_m	k_{cat} (min^{-1})	K_m (mM)	k_{cat}/K_m	E^g
SgcF wild-type	7.5 ± 0.7	2.8 ± 1.1	2.68	48 ± 3	0.89 ± 0.41	53.9	20.1
SgcF (W236Y)[a]	16 ± 1	0.041 ± 0.063	400	35 ± 10	0.92 ± 0.85	38.0	−10.5
SgcF (Q237M)	ND[b]	ND[b]	~0.04[c]	3.2 ± 0.2	4.1 ± 0.8	0.78	19.5
SgcF (W236Y/Q237M)[d]	11.3 ± 0.6	0.031 ± 0.034	355	3.3 ± 1	6.3 ± 3.1	0.52	−677
NcsF2[e]	133 ± 4	0.5 ± 0.1	266	31 ± 2	5.0 ± 0.6	6.0	−44
KedF[f]	35 ± 2.4	3.5 ± 0.64	10.0	36.6 ± 1.1	0.91 ± 0.1	40.2	4.0
SpoF	3.4 ± 0.4	2.8 ± 0.9	1.25	34 ± 3	1.1 ± 0.6	32.3	25.8
SgrF	7.9 ± 0.6	2.6 ± 0.6	3.11	43 ± 4	0.88 ± 0.45	48.9	15.7

[a]Best fit parameters to a modified Michaelis−Menten equation including substrate inhibition for (*R*)-4 (K_i = 38 mM) and (*S*)-4 (K_i = 26 mM). [b]Not determined (ND). [c]The estimate is based on the apparent linearity of the initial rate versus substrate concentration plot. [d]Best fit parameters to a modified Michaelis−Menten equation including substrate inhibition for (*R*)-4 (K_i = 20 mM) and (*S*)-4 (K_i = 18 mM). [e]Values obtained from ref 20. [f]Values obtained from ref 21. [g]Refer to the enantioselectivity $[k_{cat}/K_m(\text{fast})]/[k_{cat}/K_m(\text{slow})]$ where for positive values (*S*)-4 is the preferred (fast) substrate and for negative values (*R*)-4 is faster.

which SgcF can accommodate NcsF2-like mutations, suggests that SgcF evolved from an NcsF2-like ancestor.

We next kinetically characterized each enzyme to examine the effects of the mutations in more detail (Table 2, Figure S3). Steady-state kinetic parameters of each variant toward (*R*)- and (*S*)-**4** were determined using a previously described colorimetric assay[19] and are reported in Table 2. Although the W236Y mutation had little effect on the kinetic parameters toward (*S*)-**4**, it significantly increased k_{cat} (2-fold) and decreased K_m (70-fold) to produce a 150-fold increase in k_{cat}/K_m toward (*R*)-**4**. Thus, this single mutation switched the enantioselectivity of SgcF from an S to R preference (Figure 4). In contrast, the Q237M mutation depleted the activity toward both enantiomers to maintain the overall enantioselectivity of the wild-type enzyme. Interestingly, the W236Y/Q237M variant maintained the lower specificity of Q237M toward (*S*)-**4** and the elevated specificity of W236Y toward (*R*)-**4** to elicit a further 60-fold increase in R selectivity relative to that of the W236Y enzyme. Taken together, the results of the kinetic analyses demonstrate a trend toward increasing "NcsF2 like" behavior as NcsF2-like mutations are acquired in SgcF (Figure 5) and reveal the influence on substrate selectivity that these mutations impart on enediyne biosynthesis-associated EHs.

Despite the clear effects of these mutations on regio- and enantioselectivity, our results show that they are only partially responsible, and the complete suite of mutations capable of refashioning the active site remains to be identified. For example, although the SgcF (W236Y) mutation imparts NcsF2-like enantioselectivity, KedF possesses the same YM sequence as NcsF2 but the opposite enantioselectivity (Table 2). Thus, active-site features other than these residues are responsible for directing enantioselectivity in KedF versus NcsF2, and the unusual (*R*)-**4** preference of NcsF2 may reflect the different shape of the putative NcsF2 enediyne substrate resulting from the additional adjacent epoxide[20] (Figure 2).

Tryptophan Residue Can Predict EH Regioselectivity and Enediyne Stereochemistry. The biochemical characterization revealed that the W236Y and W236Y/Q237M variants possessed the most perturbed regioselectivity toward (*S*)-**4**, which is the enantiomer proposed to be the most biosynthetically relevant as a substrate mimic. Therefore, we set out to search for enediyne biosynthesis-associated EHs possessing this tyrosine-to-tryptophan substitution to characterize their regioselectivity and test if this mutation can predict inverting activity. A BLAST search of the NCBI database produced many (~20) hits with high sequence identity (>50%) to SgcF, and the top three hits were EHs from strains known to possess enediyne biosynthetic genes: *Streptomyces griseus* IFO 13 350 (SgrF, 72% identity),[23] *Salinospora tropica* CNB-440 (SpoF, 70% identity),[22] and NcsF2 (62% identity). Interestingly, both SgrF and SpoF possess the Y-to-W mutation: SgrF has the identical WQ motif observed in SgcF, and SpoF has WR (Figure S1).

The regioselectivities of the predicted inverting enzymes SgrF and SpoF were then assessed biochemically. The genes encoding SgrF and SpoF were cloned from *S. griseus* IFO 13 350 and *S. tropica* CNB-440, respectively, and purified His_6-tagged enzymes were obtained by Ni-affinity chromatography (Figure S2B). As expected, both enzymes catalyzed the stereochemical inversion of (*S*)-**4** to afford (*R*)-**5** in very high enantiomeric purity (Figure 3C). Moreover, steady-state kinetic parameters of both enzymes were very similar to those obtained for SgcF, with ~20-fold preference for the (*S*)-enantiomer of **4** (Table 2). We have correctly predicted EH regioselectivity on the basis of the presence of a single mutation.

Because vicinal diol stereochemistry of nine-membered enediyne cores is a consequence of EH regioselectivity, our predictive model for the latter can be extended to predict the former. Specifically, our current data indicates that inverting EHs (SgcF, SgrF, and SpoF) generate enediyne cores featuring a (*R*)-vicinal diol, and the more typical (i.e., containing two tyrosines) retaining EHs (NcsF2 and KedF) yield (*S*)-vicinal diols. Fortuitously, the gene for the inverting SpoF enzyme is located within the biosynthetic gene cluster encoding sporolides A and B, which are polycyclic macrolides proposed to arise from a nine-membered enediyne precursor containing an (*R*)-vicinal diol.[22,28] This further supports our predictive model linking EH gene sequence to the vicinal diol stereochemistry of nine-membered enediyne cores.

Phylogenetic Analysis Provides a Familial Classification of Inverting and Retaining EHs. Although the tyrosine-to-tryptophan substitution appears to play a role in directing regioselectivity, it is clearly not the only determinant. To assess if the overall EH protein sequences can be classified as inverting or retaining without specific knowledge of this mutation, we employed phylogenetic analysis on bona fide inverting (SgcF, SgrF, and SpoF) and retaining (NcsF2 and KedF) enzymes. The results demonstrate that (i) EHs associated with enediyne biosynthesis cluster together within the larger family of EHs for which extensive phylogenetic analysis has been done[26] (Figure

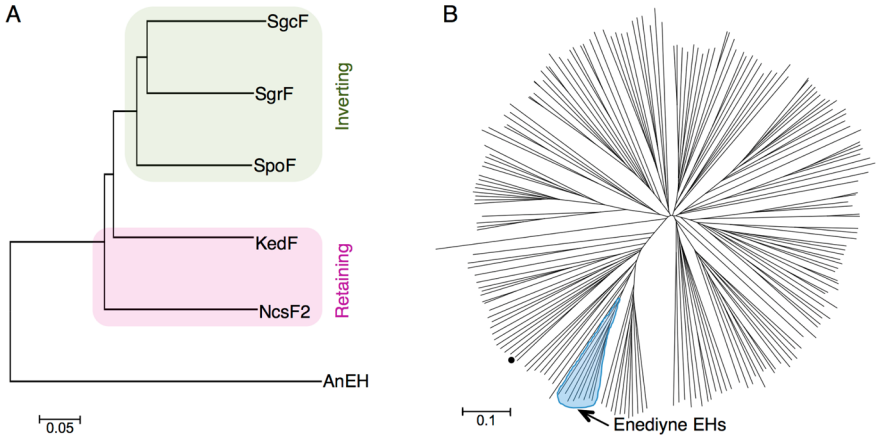

Figure 6. Phylogenetic analyses of EHs. (A) Biochemically characterized enediyne-associated EHs in a phylogram rooted with AnEH. (B) Unrooted phylogram of diverse EHs, including enediyne-associated EHs, constructed from sequences used previously.[26] AnEH is denoted by the black-filled circle. A complete list of sequences can be found in the Supporting Information.

6B) and (ii) these enediyne biosynthesis-associated EHs can be classified according to their inverting or retaining activity (Figure 6A). Taken together with the biochemical data, this strongly suggests that EH sequences can be used to predict inverting or retaining activity and therefore the respective (*R*)- or (*S*)-vicinal diol stereochemistry of nine-membered enediyne cores.

Implications for Unknown Enediynes. The *S. griseus* IFO 13 350 genome[23] possesses a cluster of enediyne biosynthetic genes including the five-gene enediyne cassette (*pksE, E3, E4, E5*, and *E10*) that is absolutely conserved among all enediyne clusters sequenced to date.[10−14,17,18,21] This cluster most probably encodes for the production of a nine-membered enediyne because it harbors genes that are apparently conserved among only nine-membered enediynes (e.g., *E2, E6-E9*, and *E11*), and the SgrF enzyme is phylogenetically clustered with other EHs that are all associated with nine-membered enediyne biosynthesis. The location of the *sgrF* gene, ∼15 kb from *pksE*, is consistent with the location of SgcF, NcsF2, and KedF within their respective gene clusters, and *sgrF* is flanked by nearby genes with homology to those from nine-membered enediyne clusters such as *mdpL* and *mdpD2*. Thus, together with our results showing that *sgrF* is biochemically and phylogenetically an inverting EH, we predict that the enediyne product from *S. griseus* IFO 13 350 is a nine-membered enediyne possessing an (*R*)-vicinal diol.

■ CONCLUSIONS

We have presented a predictive model that links the gene sequence to the molecular structure in nine-membered enediyne biosynthetic machinery. EHs from enediyne biosynthetic gene clusters can be phylogenetically classified as retaining or inverting (Figure 6A), and the latter activity originates in part from the unusual loss of one of the two tyrosines that are conserved among EHs of the α/β-hydrolase fold family. In addition, for all EHs characterized that are associated with production of a known compound, inverting and retaining EHs generate the (*R*)- and (*S*)-vicinal diols of enediyne cores, respectively. This model allows us to predict that *S. griseus* IFO 13 350 may produce an enediyne core featuring a (*R*)-vicinal diol and will no doubt aid in the structure prediction of enediynes discovered from future genome-sequencing projects. Finally, these studies provide a model system with which to study the molecular determinants of EH regioselectivity in greater detail.

■ ASSOCIATED CONTENT

Supporting Information

Summaries of all primers and plasmids, sequence homology and alignment among the five enediyne biosynthesis-associated EHs, EH sequences used to construct the phylogram, confirmation of the homogeneity of the EHs, and steady-state-kinetic analyses of the EHs with (*R*)- and (*S*)-styrene oxide as substrates. This material is available free of charge via the Internet at http://pubs.acs.org.

■ AUTHOR INFORMATION

Corresponding Author

*Tel: (561) 228-2456. Fax: (561) 228-2472. E-mail: shenb@scripps.edu.

Present Address

⊥Department of Chemistry, Wilfrid Laurier University, Waterloo, Ontario N2L 3C5, Canada.

Funding

This work was supported in part by the National Institutes of Health grants GM085770 (to B.S.M) and CA78747 (to B.S.). G.P.H. is a Natural Sciences and Engineering Research Council of Canada (NSERC) postdoctoral fellow.

Notes

The authors declare no competing financial interests.

■ ABBREVIATIONS

EH, epoxide hydrolase; KED, kedarcidin; NCS, neocarzinostatin

■ REFERENCES

(1) Bode, H. B., and Müller, R. (2005) The impact of bacterial genomics on natural product research. *Angew. Chem., Int. Ed. 44*, 6828−6846.

(2) Cox, R., Piel, J., Moore, B. S., and Weissman, K. J. (2009) Editorial: genomics themed issue. *Nat. Prod. Rep. 26*, 1353−1508.

(3) Walsh, C. T., and Fischbach, M. A. (2010) Natural products version 2.0: connecting genes to molecules. *J. Am. Chem. Soc. 132*, 2469−2493.

(4) Palmer, D. R. J., Garrett, J. B., Sharma, V., Meganathan, R., Babbitt, P. C., and Gerlt, J. A. (1999) Unexpected divergence of

enzyme function and sequence: "N-acylamino acid racemase" is o-succinylbenzoate synthase. *Biochemistry 38*, 4252−4258.
(5) Van Lanen, S. G., Lin, S., and Shen, B. (2008) Biosynthesis of the enediyne antitumor antibiotic C-1027 involves a new branching point in chorismate metabolism. *Proc. Natl. Acad. Sci. U.S.A. 105*, 494−499.
(6) Galm, U., Hager, M. H., Van Lanen, S. G., Ju, J., Thorson, J. S., and Shen, B. (2005) Antitumor antibiotics: bleomycin, enediynes, and mitomycin. *Chem. Rev. 105*, 739−758.
(7) Maeda, H. (2001) SMANCS and polymer-conjugated macromolecular drugs: advantages in cancer chemotherapy. *Adv. Drug Delivery Rev. 46*, 169−185.
(8) Nicolaou, K. C., and Dai, W. M. (1991) Chemistry and biology of the enediyne anticancer antibiotics. *Angew. Chem., Int. Ed. Engl. 30*, 1387−1416.
(9) Sievers, E. L., and Linenberger, M. (2001) Mylotarg: antibody-targeted chemotherapy comes of age. *Curr. Opin. Oncol. 13*, 522−527.
(10) Gao, Q., and Thorson, J. S. (2008) The biosynthetic genes encoding for the production of the dynemicin enediyne core in *Micromonospora chersina* ATCC53710. *FEMS Microbiol. Lett. 282*, 105−114.
(11) Ahlert, J., Shepard, E., Lomovskaya, N., Zazopoulos, E., Stafa, A., Bachmann, B. O., Huang, K., Fonstein, L., Czisny, A., Whitwam, R. E., Farnet, C. M., and Thorson, J. S. (2002) The calicheamicin gene cluster and its iterative type I enediyne PKS. *Science 297*, 1173−1176.
(12) Liu, W., Christenson, S. D., Standage, S., and Shen, B. (2002) Biosynthesis of the enediyne antitumor antibiotic C-1027. *Science 297*, 1170−1173.
(13) Liu, W., Nonaka, K., Nie, L., Zhang, J., Christenson, S. D., Bae, J., Van Lanen, S. G., Zazopoulos, E., Farnet, C. M., Yang, C. F., and Shen, B. (2005) The neocarzinostatin biosynthetic gene cluster from *Streptomyces carzinostaticus* ATCC 15944 involving two iterative type I polyketide synthases. *Chem. Biol. 12*, 293−302.
(14) Van Lanen, S. G., Oh, T.-J., Liu, W., Wendt-Pienkowski, E., and Shen, B. (2007) Characterization of the maduropeptin biosynthetic gene cluster from *Actinomadura madurae* ATCC 39144 supporting a unifying paradigm for enediyne biosynthesis. *J. Am. Chem. Soc. 129*, 13082−13094.
(15) Liang, Z.-X. (2010) Complexity and simplicity in the biosynthesis of enediyne natural products. *Nat. Prod. Rep. 27*, 499−528.
(16) Van Lanen, S. G., and Shen, B. (2008) Biosynthesis of enediyne antitumor antibiotics. *Curr. Top. Med. Chem. 8*, 448−459.
(17) Horsman, G. P., Chen, Y., Thorson, J. S., and Shen, B. (2010) Polyketide synthase chemistry does not direct biosynthetic divergence between 9- and 10-membered enediynes. *Proc. Natl. Acad. Sci. U.S.A. 107*, 11331−11335.
(18) Liu, W., Ahlert, J., Gao, Q., Wendt-Pienkowski, E., Shen, B., and Thorson, J. S. (2003) Rapid PCR amplification of minimal enediyne polyketide synthase cassettes leads to a predictive familial classification model. *Proc. Natl. Acad. Sci. U.S.A. 100*, 11959−11963.
(19) Lin, S., Horsman, G. P., Chen, Y., Li, W., and Shen, B. (2009) Characterization of the SgcF epoxide hydrolase supporting an (R)-vicinal diol intermediate for enediyne antitumor antibiotic C-1027 biosynthesis. *J. Am. Chem. Soc. 131*, 16410−16417.
(20) Lin, S., Horsman, G. P., and Shen, B. (2010) Characterization of the epoxide hydrolase NcsF2 from the neocarzinostatin biosynthetic gene cluster. *Org. Lett. 12*, 3816−3819.
(21) Lohman, J. R., Huang, S.-X., Horsman, G. P., Dilfer, P. E., Huang, T., Chen, Y., Wendt-Pienkowski, E., and Shen, B. (2013) Cloning and sequencing of the kedarcidin biosynthetic gene cluster from *Streptoalloteichus* sp. ATCC 53650 revealing new insights into biosynthesis of the enediyne family of antitumor antibiotics. *Mol. BioSyst. 9*, 478−491.
(22) Udwary, D. W., Zeigler, L., Asolkar, R. N., Singan, V., Lapidus, A., Fenical, W., Jensen, P. R., and Moore, B. S. (2007) Genome sequencing reveals complex secondary metabolome in the marine actinomycete *Salinispora tropica*. *Proc. Natl. Acad. Sci. U.S.A. 104*, 10376−10381.
(23) Ohnishi, Y., Ishikawa, J., Hara, H., Suzuki, H., Ikenoya, M., Ikeda, H., Yamashita, A., and Horinouchi, S. (2008) Genome sequence of the streptomycin-producing microorganism Streptomyces griseus IFO 13350. *J. Bacteriol. 190*, 4050−4060.
(24) Hall, B. G. (2013) Building phylogenetic trees from molecular data with MEGA. *Mol. Biol. Evol. 30*, 1229−1235.
(25) Kiefer, F., Arnold, K., Künzli, M., Bordoli, L., and Schwede, T. (2009) The SWISS-MODEL repository and associated resources. *Nucleic Acids Res. 37*, D387−392.
(26) van Loo, B., Kingma, J., Arand, M., Wubbolts, M. G., and Janssen, D. B. (2006) Diversity and biocatalytic potential of epoxide hydrolases identified by genome analysis. *Appl. Environ. Microbiol. 72*, 2905−2917.
(27) Schiøtt, B., and Bruice, T. C. (2002) Reaction mechanism of soluble epoxide hydrolase: insights from molecular dynamics simulations. *J. Am. Chem. Soc. 124*, 14558−14570.
(28) McGlinchey, R. P., Nett, M., and Moore, B. S. (2008) Unraveling the biosynthesis of the sporolide cyclohexenone building block. *J. Am. Chem. Soc. 130*, 2406−2407.
(29) Gawley, R. E. (2006) Do the terms "% ee" and "% de" make sense as expressions of stereoisomer composition or stereoselectivity? *J. Org. Chem. 71*, 2411−2416.
(30) Lindberg, D., Ahmad, S., and Widersten, M. (2010) Mutations in salt-bridging residues at the interface of the core and lid domains of epoxide hydrolase StEH1 affect regioselectivity, protein stability and hysteresis. *Arch. Biochem. Biophys. 495*, 165−173.